Published in final edited form as:

J Infect Dis. 2023 November 15; 228(Suppl 7): S536–S547. doi:10.1093/infdis/jiad136.

Fluorescent and Bioluminescent Reporter Mouse-Adapted Ebola Viruses Maintain Pathogenicity and Can Be Visualized in Vivo

Katherine A. Davies,
Stephen R. Welch,
Shilpi Jain,
Teresa E. Sorvillo,
JoAnn D. Coleman-McCray,
Joel M. Montgomery,
Christina F. Spiropoulou,
César Albariño,
Jessica R. Spengler

Viral Special Pathogens Branch, Division of High-Consequence Pathogens and Pathology, Centers for Disease Control and Prevention, Atlanta, Georgia

Abstract

Ebola virus (EBOV) causes lethal disease in humans but not in mice. Here, we generated recombinant mouse-adapted (MA) EBOVs, including 1 based on the previously reported serially adapted strain (rMA-EBOV), along with single-reporter rMA-EBOVs expressing either fluorescent (ZsGreen1 [ZsG]) or bioluminescent (nano-luciferase [nLuc]) reporters, and dual-reporter rMA-EBOVs expressing both ZsG and nLuc. No detriment to viral growth in vitro was seen with inclusion of MA-associated mutations or reporter proteins. In CD-1 mice, infection with MA-EBOV, rMA-EBOV, and single-reporter rMA-EBOVs conferred 100% lethality; infection with dual-reporter rMA-EBOV resulted in 73% lethality. Bioluminescent signal from rMA-EBOV expressing nLuc was detected in vivo and ex vivo using the IVIS Spectrum CT. Fluorescent signal from rMA-EBOV expressing ZsG was detected in situ using handheld blue-light transillumination and ex vivo through epi-illumination with the IVIS Spectrum CT. These data support the use of reporter MA-EBOV for studies of Ebola virus in animal disease models.

Correspondence: Jessica R. Spengler, DVM, PhD, MPH, 1600 Clifton Road NE, MS H18-SB, Atlanta, GA 30329 (wsk7@cdc.gov).

Supplementary Data

Supplementary materials are available at *The Journal of Infectious Diseases* online. Consisting of data provided by the authors to benefit the reader, the posted materials are not copy-edited and are the sole responsibility of the authors, so questions or comments should be addressed to the corresponding author.

Disclaimer. The findings and conclusions in this report are those of the authors and do not necessarily represent the official position of the CDC.

Potential conflicts of interest. No reported conflicts of interest. All authors have submitted the ICMJE Form for Disclosure of Potential Conflicts of Interest. Conflicts that the editors consider relevant to the content of the manuscript have been disclosed.

Keywords

filovirus; in vivo imaging; mouse-adapted Ebola virus; reporter viruses; viral hemorrhagic fever

Ebola virus (EBOV; order Mononegavirales; family Filoviridae) [1] is a single-stranded, negative-sense RNA virus. Infection results in severe, often lethal hemorrhagic fever in humans and nonhuman primates (NHPs). Most other species, including mice, are refractory to disease following infection. Mouse-adapted EBOV (MA-EBOV), developed by serial passage through progressively older mice [2], causes acute, uniform lethality in mice at low and high doses [2–4]. Viral RNA (vRNA) is widely detected in tissues, with highest levels detected in the liver and spleen and severe pathology observed in liver, spleen, and lymphoid tissues [2, 3]. Since its development, the MA-EBOV murine model has been extensively utilized to study viral pathogenesis and efficacy of medical countermeasures (MCM), including antivirals and vaccines [5].

Recombinant reporter protein–expressing viruses (reporter viruses) are valuable tools to study viruses in vitro and in vivo, including severe acute respiratory syndrome coronavirus 2 (SARS-CoV-2) [6–8], influenza [9–11], rabies [12, 13], Crimean-Congo hemorrhagic fever virus (CCHFV) [14], and Nipah virus (NiV) [15, 16]. Bioluminescence reporter virus studies have demonstrated quantification of viral infection through measurement of bioluminescent signal using in vivo optical technologies, to track and image virus localization in both serial and longitudinal studies, and to screen MCMs including vaccines [9], antivirals [12], and neutralizing antibodies [6, 9, 10]. Fluorescent reporter proteins have also been demonstrably useful to study viral pathogenesis and tissue tropism [7, 8, 14, 15]; however, most of these studies are limited to in situ or ex vivo approaches. Reporter EBOV and Marburg viruses [17–21] have been used to study filovirus pathogenesis [20, 22, 23] and in high-throughput in vitro drug screening [20–27]. However, thus far, reverse-genetics approaches to study filovirus infection using reporter proteins have been limited to wild-type, unadapted viruses only, with no reporter protein–expressing species-adapted *Ebolaviruses* available.

Here, we generated recombinant MA-EBOVs (rMA-EBOVs) expressing bioluminescent and/or fluorescent reporter proteins for use in vitro and in vivo to detect and visualize virus infection. We first characterized virus kinetics and expression of reporter proteins in vitro, then detailed infection of CD-1 mice with single- or dual-reporter–expressing rMA-EBOVs compared to parental rMA-EBOV and nonrecombinant serially adapted MA-EBOV. We describe clinical course and outcomes, as well as viral kinetics in infected mice, and confirm utility of these viruses for in vivo bioluminescent imaging, in situ fluorescent imaging, and ex vivo bioluminescent and fluorescent imaging.

METHODS

Biosafety and Ethics

All work with infectious virus or infected animals was conducted in biosafety level 4 (BSL-4) facilities at the Centers for Disease Control and Prevention (CDC; Atlanta, Georgia). Experiments involving complementary DNA encoding viral sequences were

performed in accordance with approved Institutional Biosafety Committee protocols. All animal experiments were approved by the CDC's Institutional Animal Care and Use Committee and performed in an Association for Assessment and Accreditation of Laboratory Animal Care International–approved facility.

Cells and Viruses

Vero-E6, Huh7, and BSR-T7/5 cells [28] were maintained in Dulbecco's modified Eagle medium (DMEM, Gibco) supplemented with 5% (v/v) fetal bovine serum (FBS, Cytivia) and 1× penicillin-streptomycin (Gibco). BSR-T7/5 cells were a gift from Dr K. Conzelmann (Ludwig Maximilian University of Munich). MA-EBOV strain Mayinga (CDC VirHarv #813741, GenBank AF499101.1), kindly provided by Dr Heinz Feldmann (Rocky Mountain Laboratories, National Institutes of Health), was originally generated by serial passaging in BALB/c mice [2]. Recombinant MA-EBOV and recombinant reporter strains were propagated via 1 passage in Vero-E6 cells to generate a working stock (rMA-EBOV: CDC VirHarv #815066, GenBank OQ784117; rMA-EBOV/ZsG: CDC VirHarv #815067, GenBank OQ784118; rMA-EBOV/nLuc: CDC VirHarv #815068, GenBank OQ784119; rMA-EBOV/ZsGnLuc (Zn): CDC VirHarv #815069, GenBank OQ784121; rMA-EBOV/nLucZsG (nZ): CDC VirHarv #815070, GenBank OQ784120). All working stocks were verified by next-generation sequencing (NGS) and confirmed to be mycoplasma free using MycoAlert *Mycoplasma* detection kit (Lonza).

Rescue of Recombinant Viruses

RNA from MA-EBOV Mayinga strain was used as a reverse-transcription polymerase chain reaction (RT-PCR) template to generate a full-length clone into a T7 transcription vector. The full-length clone was later modified to introduce (independently or together) 2 different reporter genes, ZsGreen1 (ZsG, Clontech) and nano-luciferase (nLuc, Promega), using InFusion cloning technology (Takara Bio). Recombinant MA-EBOV strain Mayinga viruses were rescued using support plasmids previously constructed for rescue of recombinant EBOV strain Makona [29]. Rescue events were confirmed by immunostaining infected cell monolayers or by monitoring expression of reporter genes. All recombinant viruses were sequenced by NGS; the viral genomic sequences were identical to those in the full-length plasmids.

RNA Extraction

RNA was extracted from cell culture supernatants, tissue (approximately 1 mm^3 section) homogenized in 1 mL of MagMax lysis buffer concentrate, or whole blood (50 μL) collected in lithium heparin and added to 500 μL of MagMax lysis buffer concentrate using MagMax-96 Total RNA isolation kit (Thermo Fisher Scientific) on a 96-well ABI MagMax extraction platform. Samples were treated with DNase-1 (Lucigen) and eluted into 75 μL elution buffer.

Quantitative RT-PCR

RNA was quantified using a quantitative RT-PCR (RT-qPCR) assay targeting EBOV nucleoprotein (NP). RNA quantified from harvested tissue was standardized with RT-qPCR

assays targeting *Ppia* and *Gusb*. All RT-qPCRs were carried out using SuperScript III Platinum One-Step RT-qPCR kit (Thermo Fisher Scientific). Genome copies per microliter of extracted RNA were calculated using a standard curve of an RNA oligo specific for EBOV NP diluted to known copy numbers.

Virus Quantification

Infectious virus was quantified from cell culture supernatants or from tissues (approximately 1 mm^3 section) homogenized in 1 mL DMEM supplemented with 2 × antibiotic-antimycotic (Gibco) and clarified by centrifugation at 500*g* for 10 minutes using 50% tissue culture infective dose ($TCID_{50}$) on Vero-E6 cells using the Reed-Muench method. Titers were determined by ZsG fluorescence or by indirect immunofluorescence, in which fixed cell monolayers were permeabilized using 0.1% Triton X-100 and probed using pooled polyclonal rabbit anti-Ebola serum (CDC SerHarv #703371).

Growth Kinetics in Cell Culture

Vero-E6 and Huh7 cells were seeded at 1×10^4 cells/mL onto tissue culture-treated multi-well plates 18 hours before use. Cell culture supernatants were removed, and cell monolayers were inoculated at multiplicity of infection (MOI) 1. Inoculum was removed after 1 hour absorption at 37°C and replaced with either DMEM or FluoroBrite DMEM (to assess fluorescence or bioluminescence) containing 5% FBS. Cell culture supernatants were harvested every 24 hours up to 7 days postinfection (dpi) and virus levels were quantified either by $TCID_{50}$ or by RT-qPCR. Samples were collected in triplicate, with 2 replicate analyses carried out for each sample by RT-qPCR. At equivalent time points, to measure ZsG and nLuc expression, fluorescence and bioluminescence were detected using Synergy H1 multimodal microplate reader (BioTek). Nano-Glo Luciferase Assay system (Promega) was used according to the manufacturer's instructions to induce bioluminescent signal from nLuc. Fluorescent readings were taken from 15 individual replicates and bioluminescent readings were taken from 6 individual replicates.

Immunoblotting

Vero-E6 cells were seeded and infected with rMA-EBOV at MOI 0.1, as previously described. At 7 dpi, cell culture supernatants were removed and cell lysates were harvested using 100 μL Laemmli Sample Buffer (BioRad) supplemented with 25 units Pierce Universal Nuclease (Thermo Fisher). Cell lysates were separated by sodium dodecyl sulphate–poly-acrylamide gel electrophoresis, transferred to a nitrocellulose membrane, and probed for EBOV NP and VP40, nLuc, and ZsG (Supplementary Methods).

Mouse Studies

Groups of male and female Hsd:ICR(CD-1) mice (n = 7–8; 6 weeks old; Envigo 3007M and 3006F) were inoculated intraperitoneally (IP) with a target dose of 1000 $TCID_{50}$ of the indicated MA-EBOV strains (200 μL total volume, split bilaterally). In addition, a mock-infected control group of male and female mice (n = 6) were inoculated IP as above with DMEM, and a group of male and female mice (n = 8) were inoculated subcutaneously (SC; 200 μL total volume in dorsum) with a target dose of 1000 $TCID_{50}$ MA-EBOV.

Actual dose was determined by back-titrating inoculum on Vero cells: MA-EBOV, 693 $TCID_{50}$; rMA-EBOV, 1020 $TCID_{50}$; rMA-EBOV/nLuc, 1170 $TCID_{50}$; rMA-EBOV/ZsG, 348 $TCID_{50}$; rMA-EBOV/nZ, 768 $TCID_{50}$; and rMA-EBOV/Zn, 1050 $TCID_{50}$. Animals were humanely euthanized with isoflurane vapors when endpoint criteria were reached (clinical score ≥10) or at study completion (14 dpi).

Fluorescent and Bioluminescent Imaging In Vivo and Ex Vivo

In vivo (within closed body cavity) and ex vivo (removed from body cavity) bioluminescent imaging was performed using the IVIS Spectrum CT (PerkinElmer). Mice were anesthetized using isoflurane before IP injection with 0.44 μM of Nano-Glo in vivo substrate, fluorofurimazine (Ffz) (Promega, early access material) diluted in sterile phosphate-buffered saline (200 μL total volume, split bilaterally). After 2 minutes, an intracardiac terminal blood sample was collected in lithium heparin (Sarstedt Inc) under deep isoflurane anesthesia and mice were euthanized with isoflurane vapors followed by cervical dislocation. In vivo imaging was performed 8–20 minutes after substrate injection. Following necropsy, ex vivo bioluminescent imaging was performed on liver, spleen, eyes, brain, kidneys, and reproductive and gastrointestinal tracts ≤50 minutes after substrate injection. Fluorescence was visualized and imaged in situ (within opened body cavity) as previously described using a handheld camera in conjunction with a Dark Reader camera filter and Dark Reader lamps (Clare Chemical Research, Dolores, Colorado) [14, 15]. Following necropsy, ex vivo fluorescent imaging was performed on liver, spleen, eye, brain, and reproductive tract as described above. Epi-illumination fluorescent imaging was performed on organs ex vivo using the IVIS Spectrum CT. Images were taken over multiple excitation and emission sequences; tissue autofluorescence was removed by spectral unmixing. All IVIS Spectrum CT image analysis was completed using Living Image 4.7.4 software (PerkinElmer).

Graphing and Statistical Analyses

All graphing and statistical tests were carried out in GraphPad Prism software (version 9.5.0). One-way analysis of variance was used to assess statistical differences between in vitro growth curves. Multiple unpaired *t* tests (Mann–Whitney and Kolmogorov–Smirnov) with multiple comparisons (Holm–Sidak method) were used to determine statistical differences between vRNA levels in tissues as determined by RT-qPCR. Statistical differences between survival curves were determined using the log-rank (Mantel–Cox) test.

RESULTS

Generation and Recovery of Recombinant MA-EBOV and rMA-EBOV Expressing nLuc and/or ZsG

Using reverse genetics, we generated rMA-EBOV based on the genome sequence of MA-EBOV containing the unique 13 nucleotide changes previously associated with the lethal phenotype [30]. These correspond to 8 amino acid changes and 3 silent mutations within the coding region, plus 1 insertion and 1 nucleotide change in the noncoding region [2, 30]. Variants expressing reporter proteins were generated by including nLuc and/or ZsG into the MA-EBOV genome. Single-reporter rMA-EBOVs were generated by inserting nLuc (rMA-EBOV/nLuc) or ZsG (rMA-EBOV/ZsG) coding sequence upstream of the VP40

coding sequence (Figure 1A). While including ZsG alongside VP40 of WT-EBOV has been demonstrated to minimally deter viral growth [17], the impact of including 2 reporter proteins on EBOV fitness is unknown. Thus, dual-reporter rMA-EBOV was produced using 2 strategies: inserting ZsG and nLuc coding sequences as fusion proteins upstream of the VP40 coding sequence (rMA-EBOV/Zn) or inserting ZsG and nLuc coding sequences upstream of NP and VP40, respectively (rMA-EBOV/nZ). In all variants, the self-cleaving peptide linker sequence from P2A was incorporated downstream of each reporter protein coding sequence to allow for independent expression of each individual protein (Figure 1A). All recombinant viruses were successfully rescued.

Inclusion of reporter proteins is not detrimental to in vitro growth kinetics of MA-EBOV

To determine if reporter proteins were efficiently cleaved from the associated viral protein by P2A, immunoblotting was used to evaluate expression of MA-EBOV VP40 and NP alongside ZsG and nLuc in cell lysates harvested 7 dpi from Vero-E6 cells infected at MOI 0.1 with the indicated MA-EBOV variants. ZsG and nLuc were efficiently cleaved from VP40, and nLuc was efficiently cleaved from NP. We further established that rMA-EBOV/Zn infection leads to expression of a ZsG-nLuc fusion protein, with small amounts of ZsG and nLuc also detected (Figure 1B).

To characterize viral growth kinetics of the variants, Vero-E6 and Huh7 cells were infected at MOI 1, and supernatants were harvested for virus quantification by $TCID_{50}$ and RT-qPCR every 24 hours up to 7 dpi (Figure 1C). All rMA-EBOVs demonstrated similar growth kinetics in vitro; infection in Huh7 peaked 4–5 dpi whereas titers in Vero-E6 cells continued to increase up to 7 dpi for most variants. Comparable growth kinetics were confirmed by quantifying vRNA, which demonstrated no significant difference between variants and rMA-EBOV.

To determine if reporter proteins could be used to quantify virus replication, we measured both fluorescent and luminescent signals at equivalent time points. Single- and dual-reporter rMA-EBOV strains demonstrated similar reporter protein expression patterns, with signal detection peaking 5 dpi in Vero-E6 cells and 3–4 dpi in Huh7 cells (Figure 1D).

Reporter MA-EBOVs Cause Severe or Lethal Disease in CD-1 Mice

To ensure that rMA-EBOV variants maintained the lethal phenotype in the murine model, groups of 6-week-old CD-1 mice (n = 7–8) were inoculated IP (1000 $TCID_{50}$). In addition, to confirm the nonlethal outcome previously reported for mice inoculated peripherally with MA-EBOV [2], mice (n = 8) were inoculated SC with 1000 $TCID_{50}$ of rMA-EBOV. Mice IP-infected with parental MA-EBOV or any of the rMA-EBOV variants demonstrated similar clinical signs, including weight loss, ruffled fur, hypoactivity, and ataxia, and uniformly succumbed to infection: MA-EBOV mean time to death (MTD), 5.8 days (range, 5–8 days); rMA-EBOV MTD, 5.4 days (range, 5–8 days); rMA-EBOV/nLuc MTD, 5.7 days (range, 5–6 days); and rMA-EBOV/ZsG MTD, 5.8 days (range, 5–8 days) (Figure 2A). Mice inoculated SC exhibited no clinical signs of disease and survived until study endpoint (Supplementary Figure 1).

Overall, dual-reporter strains were mildly attenuated: 11 of 15 (73%) of mice succumbed to lethal infection, 6 of 8 (75%) when infected with rMA-EBOV/nZ and 5 of 7 (71%) with rMA-EBOV/Zn. Survivors demonstrated substantial weight loss from baseline (≤15% [nZ] and ≤8% [Zn]) before returning or exceeding baseline weight by end of study. For fatal cases, MTD was 6.8 days (range, 6–10 days) for rMA-EBOV/nZ and 6.6 days (range, 6–8 days) for rMA-EBOV/Zn. No delay in onset of clinical signs was identified between non-, single-, or dual-reporter rMA-EBOV strains of EBOV (Figure 2A).

In general, vRNA levels in all tissues from mice infected with reporter rMA-EBOV demonstrated no significant differences from those detected in mice infected with parental (both rMA-EBOV and MA-EBOV) virus at terminal endpoint (Figure 2B). Infectious virus was quantified in a subset of tissues (liver, spleen, eye, brain, and reproductive tract [testis, seminal vesicle, ovary, uterus]) and detected in the majority of EBOV RT-qPCR–positive samples (Figure 2C, Supplementary Table 1). No vRNA was detected in animals surviving to study endpoint except in lungs (in 2 of 4 mice) and uterus of the single surviving female. One animal, surviving to 10 days after infection with rMA-EBOV/nZ, had detectible vRNA in the liver, kidney, and lung (Figure 2B, Supplementary Table 1). No vRNA was detected in tissue samples harvested from mock-infected controls or animals infected SC with MA-EBOV (Supplementary Table 1). ZsG and nLuc reporter proteins were genetically stable after insertion into the MA-EBOV genome; NGS revealed no mutations in the reporter protein coding sequences of EBOV RT-qPCR–positive tissue RNA from liver samples harvested at terminal endpoints (5–10 dpi) or uterine sample from a survivor at study endpoint (14 dpi).

Bioluminescent rMA-EBOV Can Be Detected In Vivo and Ex Vivo

To determine if MA-EBOV infection could be visualized non-invasively by detecting bioluminescent signal using the IVIS Spectrum CT, CD-1 mice infected with rMA-EBOV/nLuc, rMA-EBOV/nZ, or rMA-EBOV/Zn were injected with 0.44 mM Ffz nLuc substrate at terminal endpoints before imaging. Bioluminescence was detectable in animals infected with nLuc-expressing MA-EBOVs (Supplementary Table 2), with strong signal identified across the thorax and caudal abdomen and lower levels of signal detected across the dorsum and in lateral positioning. This signal was replicable across all bioluminescent reporter MA-EBOVs at terminal endpoint (Figure 3B). No bioluminescent signal was detected in vivo in control animals, animals infected with nonreporter strains of rMA-EBOV (Figure 3A), or animals that survived to endpoint after infection with dual-reporter rMA-EBOV (Supplementary Figure 2). Bioluminescence could also be detected ex vivo in the liver, spleen, and reproductive tracts of infected mice, with the strongest signal localizing to the uterine horns, ovaries, and seminal vesicles. No bioluminescence was detected in the eyes or brain (Figure 4). Though bioluminescence was not detected in vivo in rMA-EBOV/Zn survivors, it was detected ex vivo: low-level bioluminescence in the liver and seminal vesicles from the male survivor, and strong bioluminescence in the uterus of the female survivor. This uterus also tested positive for vRNA by RT-qPCR (Supplementary Figure 2, Figure 2B).

Fluorescent rMA-EBOV Can Be Visualized In Situ and Ex Vivo

In addition to detecting bioluminescence in mice infected with reporter protein–expressing rMA-EBOV, we examined whether ZsG expression could be used to visualize rMA-EBOV infection in situ and ex vivo using a handheld blue-light illumination system previously used for studying CCHFV and NiV infection [14, 15]. High fluorescence levels were seen across multiple organs in all animals infected with ZsG-expressing rMA-EBOV (Supplementary Table 2), whereas uninfected animals showed limited autofluorescence localized to the skin and urinary bladder (Figure 5A). Intense ZsG signal was detected in livers of all infected animals at terminal endpoints. Strong signal was detected in lymphoid tissues (cervical lymph nodes, thymus, Peyer patches on the intestines, and adrenal glands), pancreas, and throughout the reproductive tract in both females and males (Figure 5), whereas minimal signal was seen in kidneys, brain, and throughout the abdominal mesentery. Variable levels of ZsG signal were detected in spleen and eyes, and none in lungs or heart. Additionally, we attempted to detect ZsG expression ex situ using epi-illumination; such detection was variable, with fluorescent signal inconsistently detected across the liver, spleen, eyes, and brain. Fluorescence was detected in the reproductive tract of every animal infected with fluorescent reporter protein–expressing rMA-EBOV examined at terminal endpoint (Figure 5B).

DISCUSSION

MA-EBOV is a key tool for studying EBOV pathogenesis and evaluating MCMs in mouse models [5]. To enhance the utility of this tool, we generated recombinant reporter protein–expressing rMA-EBOV variants that maintain pathogenicity in mice and found that bioluminescent and fluorescent signals could be detected in mice infected with dual-reporter MA-EBOVs similarly to those infected with single-reporter MA-EBOVs.

Bioluminescent signals from MA-EBOV reporter viruses were readily detected at terminal endpoints in vivo and ex vivo using the IVIS Spectrum CT. Bioluminescent reporters can also be used to track viral infection in real time spatially and longitudinally, to track transmission of virus between animals [7], and to evaluate MCMs [6, 9, 10, 12]. Furthermore, some imaging modalities, such as the IVIS Spectrum CT, have the capability to perform microCT alongside bioluminescent imaging, permitting visualization of the spatial location of reporter proteins in vivo [31]. Further anatomical context of viral biodistribution can be determined by co-registering detected signal with a 3-dimensional organ atlas, as demonstrated with SARS-CoV-2 [32]; this can provide further insights into viral dissemination and infection patterns when used alongside reporter-expressing viruses.

Signal generated by ZsG fluorescent reporter-expressing rMA-EBOV was detectable in situ and ex vivo using blue-light transillumination and ex vivo using the epi-illumination. Bioluminescence can be detected from deep tissue sources whereas fluorescence detection is largely limited to organ surfaces; we found that in vivo detection of fluorescence with epi-illumination in these mice was not representative of the strength of signal detected ex vivo, nor was as strong as the bioluminescent signal from mice with similar outcomes. ZsG has an emission wavelength of approximately 500 nm, which allows visualization of infected surface organs but is readily absorbed by hemoglobin and water in tissues,

complicating detection from deeper locations [33]. Other factors impacting detection of fluorescence include tissue thickness and tissue autofluorescence signal quenching and scattering, which can im-pede detection of fluorescent signal from deep tissue [34]. Far-red or near-infrared (NIR) fluorescent proteins with wave-lengths above 650 nm (which are less absorbed by tissues) may be more readily detected, as shown with NIR-labeled rabies virus [13], although the sensitivity of NIR fluorescence was still noted to be less than that of bioluminescence [12]. Nevertheless, fluorescent reporter viruses can be used for more than visualizing sites of infection; for example, recently developed techniques such as in vivo flow cytometry may provide mechanistic insights into infection dynamics by longitudinal quantification of infected immune cells [35].

Dual-reporter MA-EBOVs exhibited mild attenuation compared to non- or single-reporter variants. Previously, a dual-reporter influenza virus was highly attenuated and nonlethal in mice [36], unlike a single reporter, which was mildly attenuated [37]. In contrast, no difference in virulence was observed during infection with single- or dual-reporter SARS-CoV-2 [7, 38] or vaccinia virus [39]. For EBOV, including a single fluorescent reporter into the VP30–VP24 intergenic region resulted in moderate attenuation of the lethal phenotype in immunocompromised mice and completely nonlethal in rhesus macaques compared to parental EBOV [40]. In our study, although dual-reporter rMA-EBOVs were not universally lethal, survivors exhibited significant clinical signs and vRNA was detected in several organs after recovery. Nonuniform lethality may offer a unique opportunity to explore and visualize factors associated with survival, recrudescence, persistence, and transmission postrecovery.

Our data provide key support for the application of single- and dual-labeled reporter viruses for studying MA-EBOV infection in the murine model. While bioluminescent imaging in live animals is limited due to size constrains of the imaging modalities and organ-to-surface distances in larger animals, it may be possible to image organs from large animal models, such as NHPs, ex vivo, as demonstrated here. Furthermore, fluorescent reporter virus–infected cells can be detected by flow cytometry [14], allowing this technology to be differentially applied to future investigations into viral pathogenesis and immunology. Finally, reverse-genetics approaches described here could be used for reporter labeling of other EBOV strains such as wild-type or guinea pig–adapted viruses that are known to be pathogenic in NHPs, permitting these types of studies in additional animal models. Overall, the reporter viruses and approaches described here provide new opportunities for advanced studies of pathogenesis and MCM evaluation.

Supplementary Material

Refer to Web version on PubMed Central for supplementary material.

Acknowledgments.

We thank Tatyana Klimova for assistance with editing the manuscript and members of the Centers for Disease Control and Prevention’s (CDC) Comparative Medicine Branch for providing care for the animals.

Financial support.

This work was supported in part by CDC Emerging Infectious Disease Research Core funds, by the American Rescue Plan Act, and by an appointment to the CDC, administered by the Oak Ridge Institute for Science and Education (ORISE) through an interagency agreement between the US Department of Energy (DOE) and the United States Department of Agriculture (USDA)-Agriculture Research Services (ARS) (to K. A. D.). ORISE is managed by Oak Ridge Associated Universities under contract with DOE.

Supplement sponsorship.

This article appears as part of the supplement "10th International Symposium on Filoviruses."

References

1. Walker PJ, Siddell SG, Lefkowitz EJ, et al. Changes to virus taxonomy and to the International Code of Virus Classification and Nomenclature ratified by the International Committee on Taxonomy of Viruses (2021). Arch Virol 2021; 166:2633–48. [PubMed: 34231026]
2. Bray M, Davis K, Geisbert T, Schmaljohn C, Huggins J. A mouse model for evaluation of prophylaxis and therapy of Ebola hemorrhagic fever. J Infect Dis 1998; 178:651–61. [PubMed: 9728532]
3. Spengler JR, Welch SR, Ritter JM, et al. Mouse models of Ebola virus tolerance and lethality: characterization of CD-1 mice infected with wild-type, guinea pig-adapted, or mouse-adapted virus. Antiviral Res 2023; 210:105496. [PubMed: 36567020]
4. Haddock E, Feldmann H, Marzi A. Ebola virus infection in commonly used laboratory mouse strains. J Infect Dis 2018; 218:S453–7. [PubMed: 29878128]
5. Bradfute SB. History and impact of the mouse-adapted Ebola virus model. Antiviral Res 2023; 210:105493. [PubMed: 36567023]
6. Ye C, Chiem K, Park JG, et al. Analysis of SARS-CoV-2 infection dynamic in vivo using reporter-expressing viruses. Proc Natl Acad Sci U S A 2021; 118:e2111593118.
7. Chiem K, Park J-G, Morales Vasquez D, et al. Monitoring SARS-CoV-2 infection using a double reporter-expressing virus. Microbiol Spectr 2022; 10:e0237922. [PubMed: 35980204]
8. Chiem K, Morales Vasquez D, Silvas JA, et al. A bifluorescent-based assay for the identification of neutralizing antibodies against SARS-CoV-2 variants of concern in vitro and in vivo. J Virol 2021; 95:e0112621. [PubMed: 34495697]
9. Czakó R, Vogel L, Lamirande EW, et al. In vivo imaging of influenza virus infection in immunized mice. mBio 2017; 8: e00714–17. [PubMed: 28559489]
10. Heaton NS, Leyva-Grado VH, Tan GS, Eggink D, Hai R, Palese P. In vivo bioluminescent imaging of influenza A virus infection and characterization of novel cross-protective monoclonal antibodies. J Virol 2013; 87:8272–81. [PubMed: 23698304]
11. Kim JH, Bryant H, Fiedler E, Cao T, Rayner JO. Real-time tracking of bioluminescent influenza A virus infection in mice. Sci Rep 2022; 12:3152. [PubMed: 35210462]
12. Yamada K, Noguchi K, Kimitsuki K, et al. Reevaluation of the efficacy of favipiravir against rabies virus using in vivo imaging analysis. Antiviral Res 2019; 172:104641. [PubMed: 31672666]
13. Isomura M, Yamada K, Noguchi K, Nishizono A. Near-infrared fluorescent protein iRFP720 is optimal for in vivo fluorescence imaging of rabies virus infection. J Gen Virol 2017; 98:2689–98. [PubMed: 29039733]
14. Welch SR, Ritter JM, McElroy AK, et al. Fluorescent Crimean-Congo hemorrhagic fever virus illuminates tissue tropism patterns and identifies early mononuclear phagocytic cell targets in Ifnar$^{-/-}$ mice. PLoS Pathog 2019; 15: e1008183. [PubMed: 31790513]
15. Welch SR, Scholte FEM, Harmon JR, et al. In situ imaging of fluorescent Nipah virus respiratory and neurological tissue tropism in the Syrian hamster model. J Infect Dis 2020; 221:S448–53. [PubMed: 31665342]
16. Escaffre O, Hill T, Ikegami T, et al. Experimental infection of Syrian hamsters with aerosolized Nipah virus. J Infect Dis 2018; 218:1602–10. [PubMed: 29912426]

17. Albariño CG, Wiggleton Guerrero L, Lo MK, Nichol ST, Towner JS. Development of a reverse genetics system to generate a recombinant Ebola virus Makona expressing a green fluorescent protein. Virology 2015; 484:259–64. [PubMed: 26122472]
18. Ebihara H, Groseth A, Neumann G, Kawaoka Y, Feldmann H. The role of reverse genetics systems in studying viral hemorrhagic fevers. Thromb Haemost 2005; 94:240–53. [PubMed: 16113812]
19. Albariño CG, Uebelhoer LS, Vincent JP, et al. Development of a reverse genetics system to generate recombinant Marburg virus derived from a bat isolate. Virology 2013; 446(1–2):230–7. [PubMed: 24074586]
20. Uebelhoer LS, Albariño CG, McMullan LK, et al. High-throughput, luciferase-based reverse genetics systems for identifying inhibitors of Marburg and Ebola viruses. Antiviral Res 2014 ; 106:86–94. [PubMed: 24713118]
21. Hoenen T, Groseth A, Callison J, Takada A, Feldmann H. A novel Ebola virus expressing luciferase allows for rapid and quantitative testing of antivirals. Antiviral Res 2013; 99:207–13. [PubMed: 23751367]
22. Warren TK, Warfield KL, Wells J, et al. Antiviral activity of a small-molecule inhibitor of filovirus infection. Antimicrob Agents Chemother 2010; 54:2152–9. [PubMed: 20211898]
23. Aman MJ, Kinch MS, Warfield K, et al. Development of a broad-spectrum antiviral with activity against Ebola virus. Antiviral Res 2009; 83:245–51. [PubMed: 19523489]
24. Towner JS, Paragas J, Dover JE, et al. Generation of eGFP expressing recombinant Zaire ebolavirus for analysis of early pathogenesis events and high-throughput antiviral drug screening. Virology 2005; 332:20–7. [PubMed: 15661137]
25. Panchal RG, Kota KP, Spurgers KB, et al. Development of high-content imaging assays for lethal viral pathogens. J Biomol Screen 2010; 15:755–65. [PubMed: 20639507]
26. Johansen LM, Brannan JM, Delos SE, et al. FDA-approved selective estrogen receptor modulators inhibit Ebola virus infection. Sci Transl Med 2013; 5:190ra79.
27. Panchal RG, Reid SP, Tran JP, et al. Identification of an antioxidant small-molecule with broad-spectrum antiviral activity. Antiviral Res 2012; 93:23–9. [PubMed: 22027648]
28. Buchholz UJ, Finke S, Conzelmann K-K. Generation of bovine respiratory syncytial virus (BRSV) from cDNA: BRSV NS2 is not essential for virus replication in tissue culture, and the human RSV leader region acts as a functional BRSV genome promoter. J Virol 1999; 73:251–9. [PubMed: 9847328]
29. Albariño CG, Guerrero LW, Chakrabarti AK, et al. Virus fitness differences observed between two naturally occurring isolates of Ebola virus Makona variant using a reverse genetics approach. Virology 2016 ; 496:237–43. [PubMed: 27366976]
30. Ebihara H, Takada A, Kobasa D, et al. Molecular determinants of Ebola virus virulence in mice. PLoS Pathog 2006 ; 2:0705–11.
31. Kuo C, Coquoz O, Troy TL, Xu H, Rice BW. Three-dimensional reconstruction of in vivo bioluminescent sources based on multispectral imaging. J Biomed Opt 2007; 12:024007. [PubMed: 17477722]
32. Carossino M, Kenney D, O'Connell AK, et al. Fatal neuro-dissemination and SARS-CoV-2 tropism in K18-hACE2 mice is only partially dependent on hACE2 expression. Viruses 2022; 14:535. [PubMed: 35336942]
33. Weissleder R A clearer vision for in vivo imaging. Nat Biotechnol 2001; 19:316–7. [PubMed: 11283581]
34. Hickson J In vivo optical imaging: preclinical applications and considerations. Urol Oncol 2009; 27:295–7. [PubMed: 19414115]
35. Tan X, Patil R, Bartosik P, Runnels JM, Lin CP, Niedre M. In vivo flow cytometry of extremely rare circulating cells. Sci Rep 2019; 9:1–11. [PubMed: 30626917]
36. Nogales A, Ávila-Pérez G, Rangel-Moreno J, Chiem K, DeDiego ML, Martínez-Sobrido L. A novel fluorescent and bioluminescent bireporter influenza A virus to evaluate viral infections. J Virol 2019 ; 93:e00032–19. [PubMed: 30867298]
37. Nogales A, Baker SF, Martínez-Sobrido L. Replication-competent influenza A viruses expressing a red fluorescent protein. Virology 2015 ; 476:206–16. [PubMed: 25553516]

38. Morales Vasquez D, Chiem K, Ye C, Martinez-Sobrido L. Bioluminescent and fluorescent reporter-expressing recombinant SARS-CoV-2. Methods Mol Biol 2022; 2524: 235–48. [PubMed: 35821476]

39. Chiem K, Lorenzo MM, Rangel-Moreno J, et al. Bi-reporter vaccinia virus for tracking viral infections in vitro and in vivo. Microbiol Spectr 2021; 9:e0160121. [PubMed: 34817228]

40. Ebihara H, Theriault S, Neumann G, et al. In vitro and in vivo characterization of recombinant Ebola viruses expressing enhanced green fluorescent protein. J Infect Dis 2007; 196:S313–22. [PubMed: 17940966]

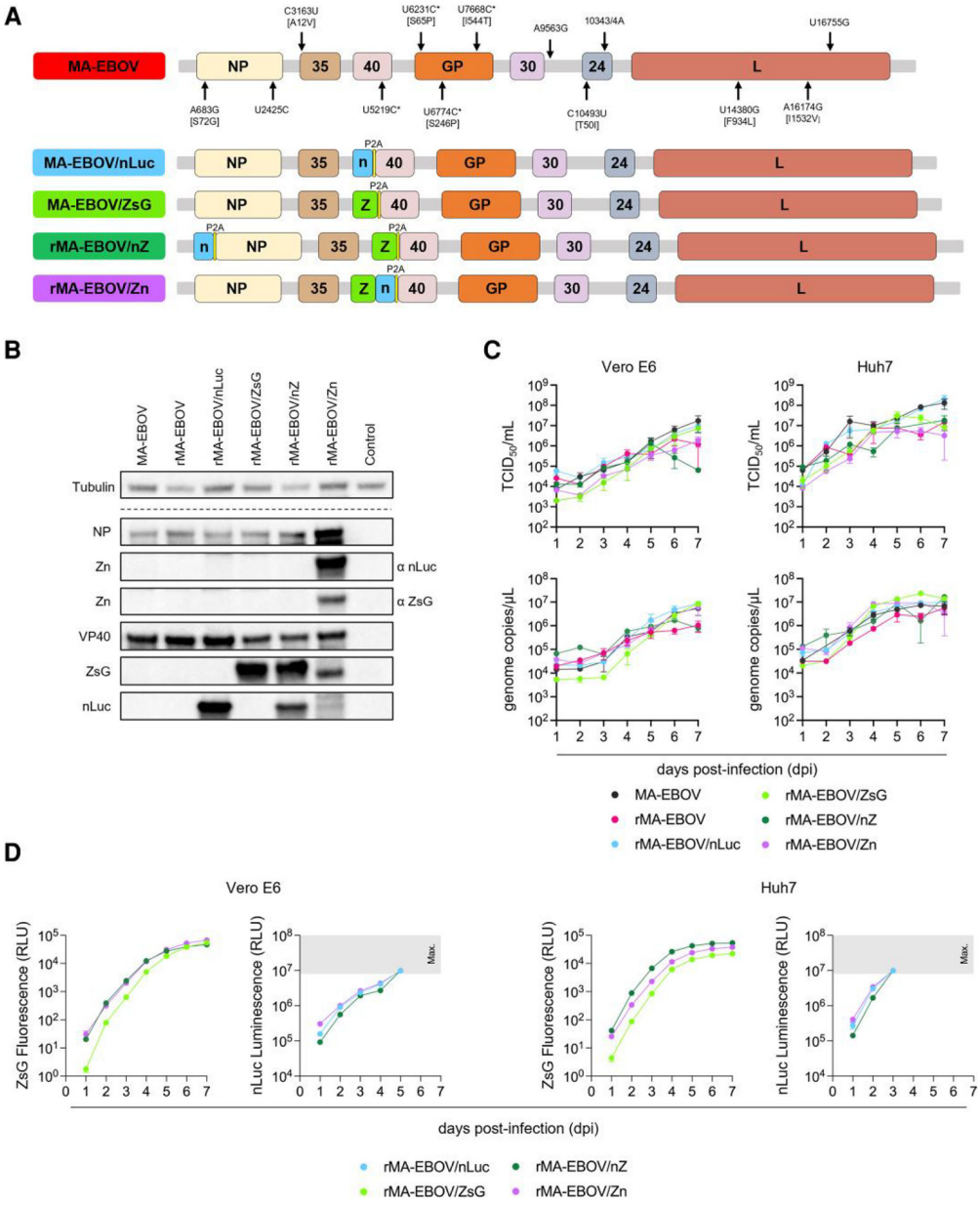

Figure 1.

Recombinant mouse-adapted Ebola viruses (rMA-EBOVs) and reporter-expressing rMA-EBOVs demonstrate similar growth kinetics in vitro. *A*, Genome schematic of MA-EBOV indicating mutations associated with lethal disease in the murine model. Asterisk (*) indicates mutations in the original precursor virus that differ from those in the published wild-type EBOV sequence (GenBank #AF086833) as indicated in [30]. Amino acid changes are indicated in brackets. Genome schematics of the recombinant reporter MA-EBOV variants are shown; location of the reporter proteins nano-luciferase (nLuc or n) and ZsGreen1 (ZsG or Z) are indicated by blue and green boxes, respectively. *B*, Cleavage efficiency of the P2A peptide was assessed by examining total cell lysates from Vero-E6 cells infected with rMA-EBOV (multiplicity of infection [MOI] 0.1) and reporter protein–

expressing rMA-EBOV variants at 7 days postinfection (dpi). Lysates were analyzed by Western blotting and probed using antibodies against EBOV nucleoprotein and VP40, and additionally against the reporter proteins ZsG and nLuc. Tubulin was included as a loading control. Expected size for each protein was as follows: nucleoprotein, ~85 kDa; tubulin, ~55 kDa; ZsG/nLuc fusion protein (Zn), ~45 kDa; VP40, ~40 kDa; ZsG, ~25 kDa; nLuc, ~20 kDa. *C*, Vero-E6 and Huh7 cells were infected with MA-EBOV, rMA-EBOV, or reporter rMA-EBOV variants (MOI 1). Cell culture supernatants were collected every 24 h up to 7 dpi. Virus was quantified via 50% tissue culture infective dose ($TCID_{50}$) determination and quantitative reverse-transcription polymerase chain reaction (RT-qPCR). Each data point is represented as the mean of 3 biological replicates, assayed in quadruplicate ($TCID_{50}$) or 3 biological replicates, assayed in duplicate (RT-qPCR). Error bars represent standard error of the mean. No significant growth differences were found between parental MA-EBOV or rMA-EBOV variants using 1-way analysis of variance. *D*, Expression of reporter proteins was assessed by detecting fluorescent and bioluminescent signal in Vero-E6 and Huh7 monolayers infected with reporter-expressing rMA-EBOVs (MOI 1.0). Monolayers were assessed every 24 h up to 7 dpi. Gray box indicates signal above the maximum detection threshold of the instrument. Each data point is represented as the mean of 15 biological replicates (ZsG) or 6 biological replicates (nLuc). Error bars represent standard error of the mean. Abbreviations: 24, VP24; 30, VP30; 35, VP35; 40, VP40; dpi, days postinfection; GP, glycoprotein; L, polymerase; MA-EBOV, mouse-adapted Ebola virus; nLuc or n, nano-luciferase; NP, nucleoprotein; nZ, nLucZsG; P2A, porcine teschovirus-1 2A self-cleaving peptide sequence; RLU, relative light unit; rMA-EBOV, recombinant mouse-adapted Ebola virus; $TCID_{50}$, 50% tissue culture infective dose; Zn, ZsGnLuc; ZsG or Z, ZsGreen1.

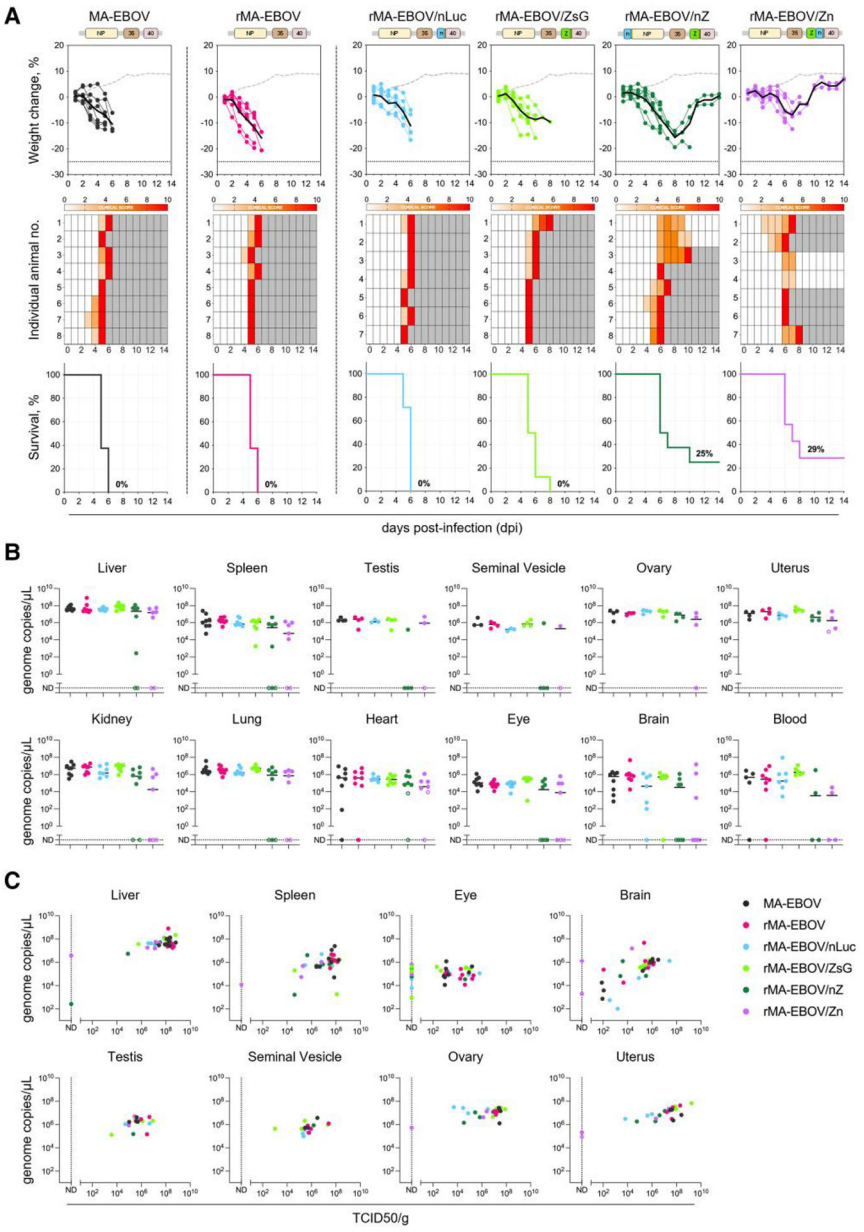

Figure 2.

Recombinant mouse-adapted Ebola virus (rMA-EBOV) and single-reporter rMA-EBOV maintain pathogenicity in vivo. *A*, Weight change from baseline (day 0), clinical signs, and survival of CD-1 mice infected intraperitoneally with 1000 $TCID_{50}$ (50% tissue culture infective dose) of either mouse-adapted Ebola virus (MA-EBOV), rMA-EBOV, or reporter protein–expressing rMA-EBOV variants. Solid black lines and dashed gray lines represent the mean weight change for virus-infected and vehicle-only mock-infected (Dulbecco's modified Eagle medium) mice, respectively. Severity of clinical signs is indicated by the color scale (1–10); gray shading indicates animal reached terminal endpoint. There was no statistical significance in % survival between mice infected with recombinant and single-reporter adapted strains when assessed using the log-rank (Mantel–Cox) test. *B*, Viral RNA

was quantified by quantitative reverse-transcription polymerase chain reaction (RT-qPCR) using primer sets specific for MA-EBOV nucleoprotein in blood and fresh tissues collected at necropsy (liver, spleen, gonad [testis or ovary], kidney, heart, lung, eye, brain); and in seminal vesicle or uterus from tissue frozen at time of collection. The median value is indicated by the black line, and closed circles indicate samples taken from animals reaching terminal endpoints; open circles indicate samples taken from animals surviving to study endpoint. There were no statistical differences in tissue viral loads (determined by RT-qPCR) between mice infected with recombinant and adapted strains when using multiple unpaired *t* tests (Mann–Whitney and Kolmogorov–Smirnov). *C*, Scatter plots depicting relationship between viral RNA loads (genome copies/μL) versus infectious virus titers ($TCID_{50}$/g) for liver, spleen, testes, seminal vesicle, ovary, uterus, eye, and brain tissue samples. Abbreviations: dpi, days postinfection; MA-EBOV, mouse-adapted Ebola virus; nLuc, nano-luciferase; nZ, nLucZsG; rMA-EBOV, recombinant mouse-adapted Ebola virus; $TCID_{50}$, 50% tissue culture infective dose; Zn, ZsGnLuc; ZsG, ZsGreen1.

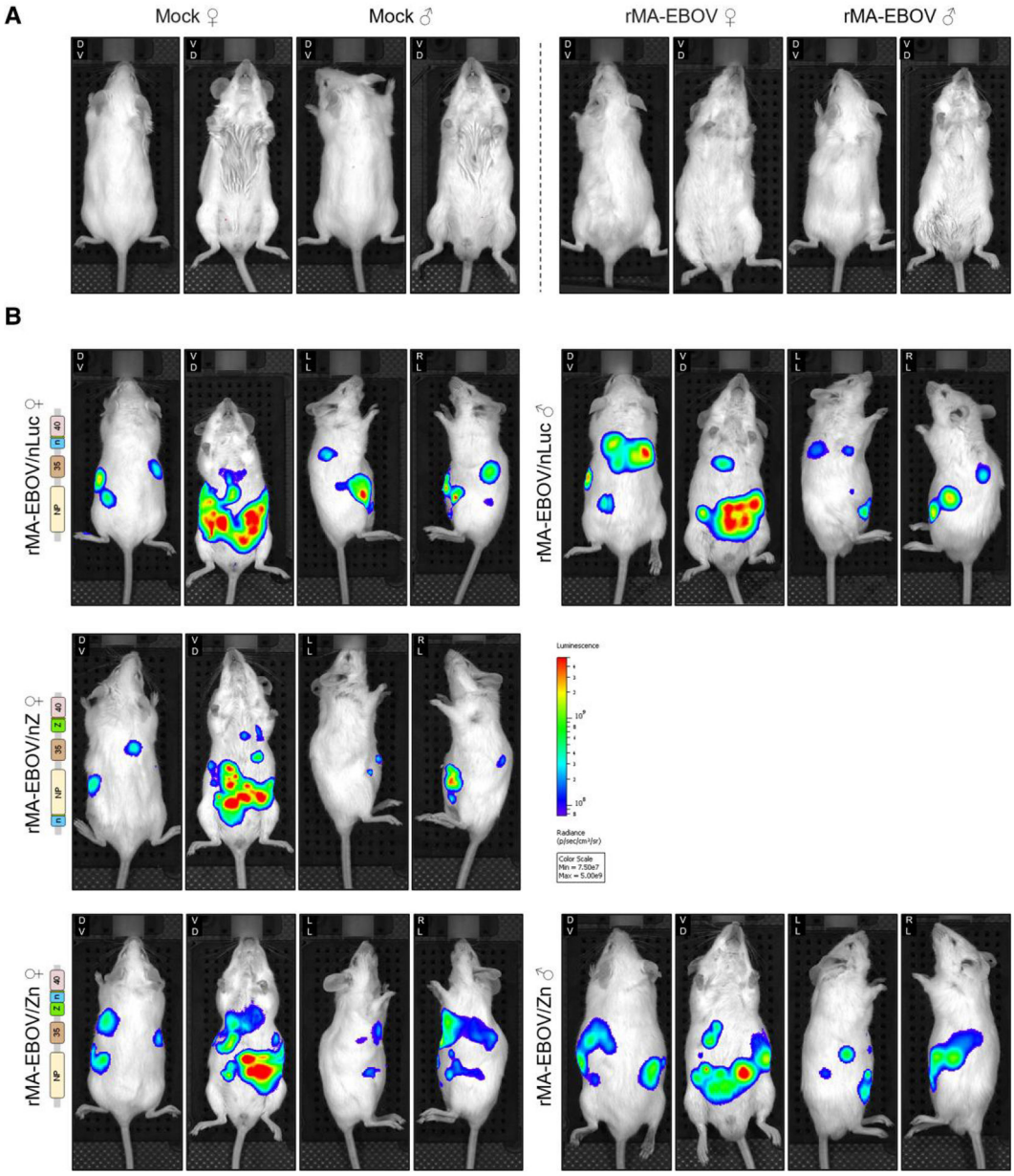

Figure 3.

nLuc signal can be visualized in vivo in mice infected with bioluminescent reporter recombinant mouse-adapted Ebola virus (rMA-EBOV) variants. CD-1 mice infected intraperitoneally with 1000 50% tissue culture infective dose ($TCID_{50}$) rMA-EBOV, rMA-EBOV/nano-luciferase (nLuc), rMA-EBOV/nZ, or rMA-EBOV/Zn at terminal endpoint, or control mock-infected animals at study endpoint, were injected with nLuc substrate (Ffz), euthanized, and examined for bioluminescence using the IVIS Spectrum CT. *A*, No bioluminescent signal was detected in control animals or those infected with nonreporter rMA-EBOV. *B*, Bioluminescent signal was detected in CD-1 mice infected with either single- or dual-reporter rMA-EBOV expressing nLuc. Relative luminescence is expressed as photons per second per square centimeter per steradian (p/sec/cm^2/sr) indicated by the color

scale. Representative and available images are shown. No images were available for male mice infected with rMA-EBOV/nZ at terminal endpoints. Abbreviations: ♀, female; ♂, male; DV, dorsoventral; LL, left lateral; nLuc, nano-luciferase; nZ, nLucZsG; RL, right lateral; rMA-EBOV, recombinant mouse-adapted Ebola virus; VD, ventrodorsal; Zn, ZsGnLuc.

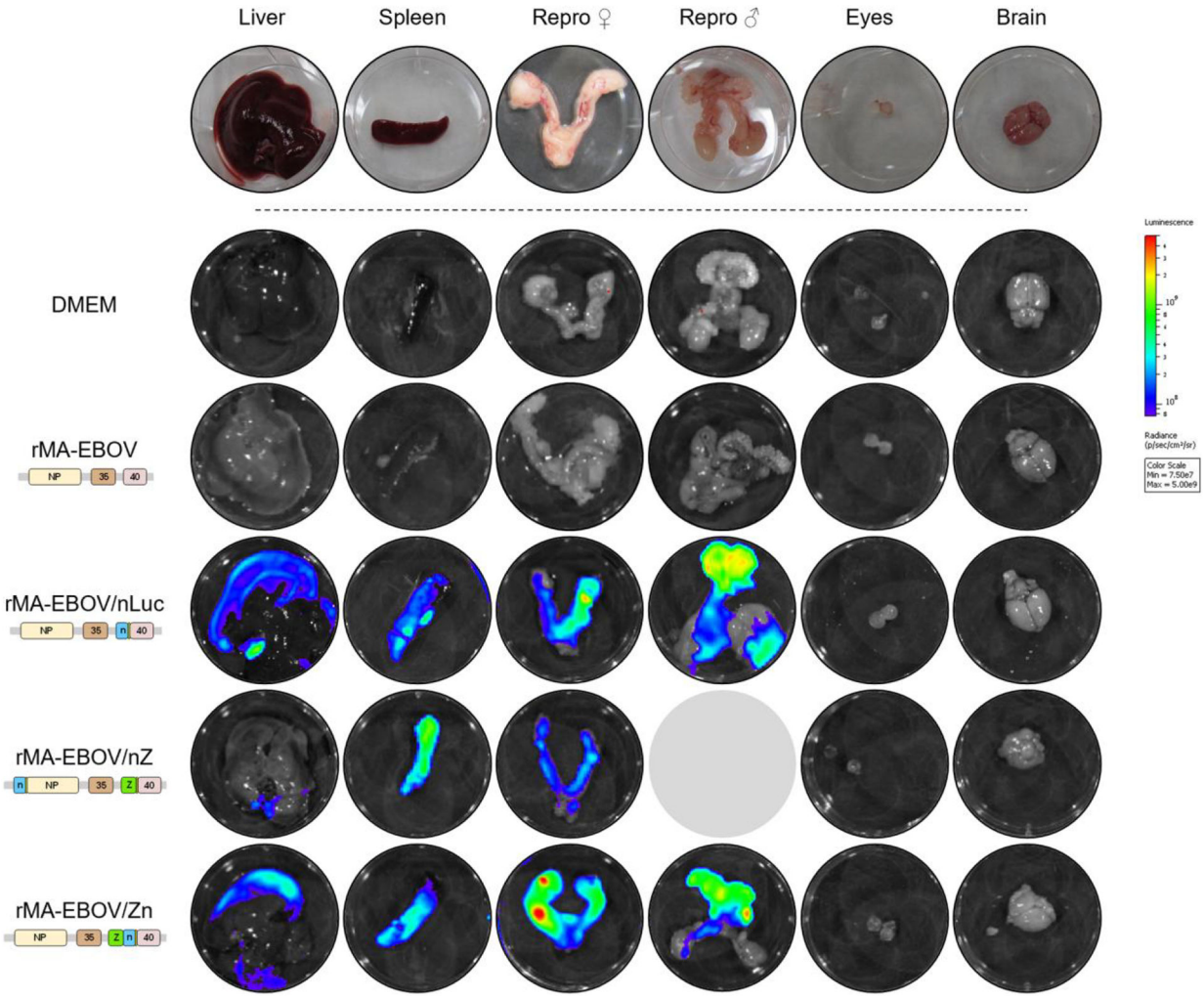

Figure 4.

Bioluminescent reporter recombinant mouse-adapted Ebola viruses (rMA-EBOVs) can be used for the ex vivo detection of MA-EBOV infection in mice. CD-1 mice infected intraperitoneally with 1000 50% tissue culture infective dose ($TCID_{50}$) rMA-EBOV, rMA-EBOV/nano-luciferase (nLuc), rMA-EBOV/nZ, or rMA-EBOV/Zn at terminal endpoint, or control mock-infected animals at study endpoint, were injected with nLuc substrate (Ffz) and euthanized. Liver, spleen, reproductive tract, eyes, and brain were excised and examined ex vivo for bioluminescence using the IVIS Spectrum CT. *A*, No signal was detected in organs harvested from control animals or those infected with nonreporter rMA-EBOV. *B*, Detection of bioluminescent signal from animals infected with nLuc-expressing rMA-EBOV. Relative luminescence is expressed as photons per second per square centimeter per steradian (p/sec/cm^2/sr) indicated by the color scale. Representative and available images are shown. No sample was available for male reproductive organs with rMA-EBOV/nZ at terminal endpoint. Abbreviations: ♀, female; ♂, male; DMEM, Dulbecco's modified Eagle medium; nLuc, nano-luciferase; NP, nucleoprotein; nZ, nLucZsG; Repro, reproductive tract; rMA-EBOV, recombinant mouse-adapted Ebola virus; Zn, ZsGnLuc.

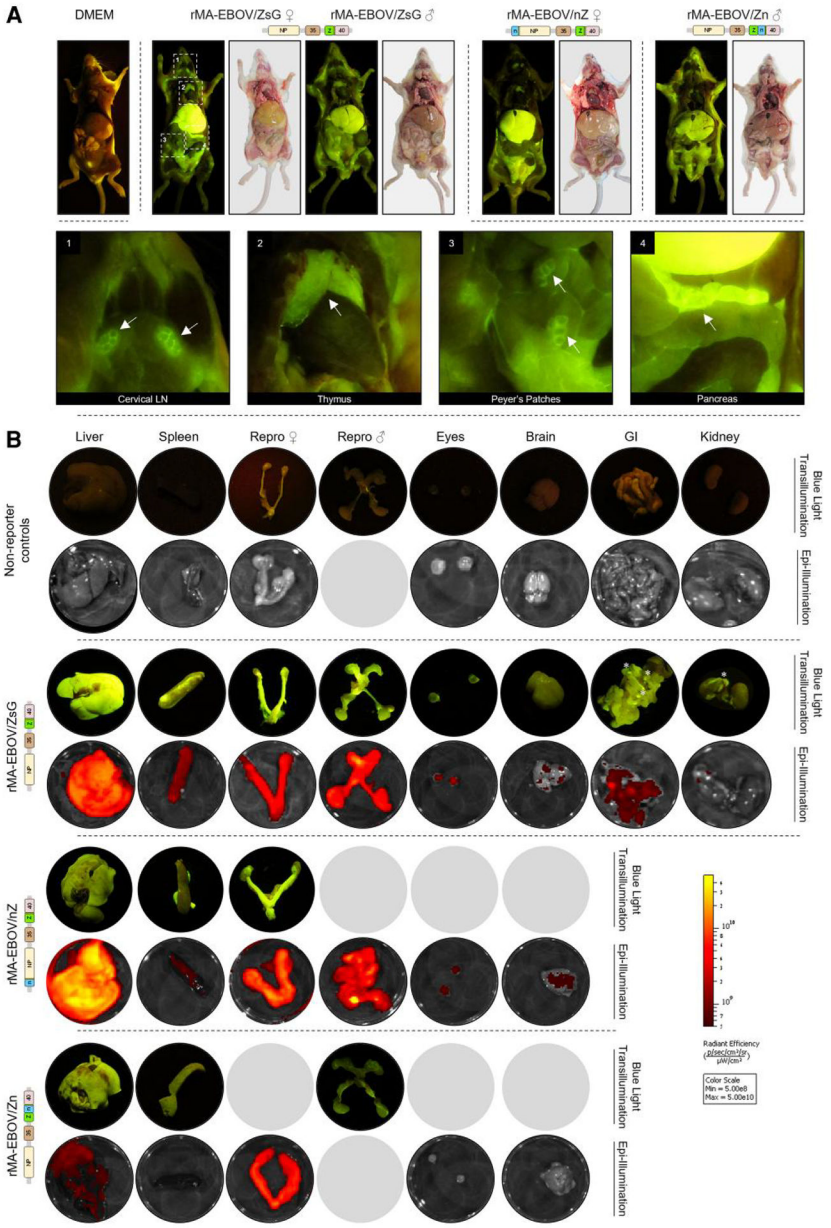

Figure 5.

ZsGreen1 (ZsG) signal can be visualized in situ and ex vivo in mice infected with fluorescent reporter protein–expressing recombinant mouse-adapted Ebola virus (rMA-EBOV) variants. CD-1 mice infected intraperitoneally with 1000 50% tissue culture infective dose rMA-EBOV/ZsG, rMA-EBOV/nZ, or rMA-EBOV/Zn were euthanized at terminal endpoints and imaged using blue-light transillumination and/or epi-illumination (IVIS Spectrum CT). In situ blue-light transillumination. ZsG expression was visualized by photographing under blue-light transillumination and white light. Control animals (far left panel) demonstrated expected autofluorescence in the urinary bladder and skin. White boxes indicate areas of interest and white arrows indicate fluorescent signal in the cervical lymph nodes (1), thymus (2), Peyer patches on the intestines (3), and pancreas (4). Ex vivo tissue

imaging. Liver, spleen, reproductive organs, eyes, and brain were removed and examined ex vivo for fluorescence by blue-light transillumination and epi-illumination. Additionally, for control animals and animals infected with rMA-EBOV/ZsG, gastrointestinal tracts and kidneys were removed and examined by blue-light transillumination and epi-illumination. Peyer patches on the intestines and adrenal gland on the kidneys are indicated with an asterisk (*). No fluorescence was detected ex vivo from control animals (Dulbecco's modified Eagle medium and rMA-EBOV) when imaged using blue-light transillumination and epi-illumination. Relative epifluorescence detected by the IVIS Spectrum CT is expressed as (photons per second per square centimeter per steradian) per (microwatt per square centimeter) ([p/sec/cm^2/sr]/[μW/cm^2]), indicated by the color scale. Representative and available images are shown. No sample of male reproductive organs from mice infected with rMA-EBOV/Zn at terminal endpoint was imaged. Abbreviations: ♀, female; ♂, male; DMEM, Dulbecco's modified Eagle medium; GI, gastrointestinal tract; LN, lymph node; NP, nucleoprotein; nZ, nLucZsG; rMA-EBOV, recombinant mouse-adapted Ebola virus; Zn, ZsGnLuc; ZsG, ZsGreen1.